Published in final edited form as:

Curr Biol. 2017 June 19; 27(12): 1791–1800.e5. doi:10.1016/j.cub.2017.05.022.

Synergistic Signaling by Light and Acetylcholine in Mouse Iris Sphincter Muscle

Qian Wang[1,3,4,†,*], **Wendy Wing Sze Yue**[1,3,4,+], **Zheng Jiang**[1,3], **Tian Xue**[5], **Shin H. Kang**[1,^], **Dwight E. Bergles**[1], **Katsuhiko Mikoshiba**[6], **Stefan Offermanns**[7], **King-Wai Yau**[1,2,3,8,*]

[1]Solomon H. Snyder Department of Neuroscience, Johns Hopkins University School of Medicine, Baltimore, MD 21205, USA

[2]Department of Ophthalmology, Johns Hopkins University School of Medicine, Baltimore, MD 21205, USA

[3]Center for Sensory Biology, Johns Hopkins University School of Medicine, Baltimore, MD 21205, USA

[4]Biochemistry, Cellular and Molecular Biology Graduate Program, Johns Hopkins University School of Medicine, Baltimore, MD 21205, USA

[5]Chinese Academy of Science Key Laboratory of Brain Function and Diseases, School of Life Sciences, University of Science and Technology of China, Hefei 230027, Anhui, PR China

[6]Laboratory for Developmental Neurobiology, RIKEN Brain Science Institute, Saitama 351-0198, Japan

[7]Max-Planck-Institute for Heart and Lung Research, 61231 Bad Nauheim, Germany

[8]Lead Contact

SUMMARY

The mammalian pupillary light reflex (PLR) involves a bilateral brain circuit whereby afferent light signals in the optic nerve ultimately drive iris-sphincter-muscle contraction via excitatory cholinergic parasympathetic innervation [1,2]. Additionally, the PLR in nocturnal and crepuscular sub-primate mammals has a “local” component in the isolated sphincter muscle [3–5], as in amphibians, fish and bird [6–10]. In mouse, this ‘local’ PLR requires the pigment melanopsin [5] originally found in intrinsically-photosensitive retinal ganglion cells (ipRGCs) [11–19]. However, melanopsin’s presence and effector pathway locally in the iris remain uncertain. The sphincter

*Correspondence: kwyau@jhmi.edu (K.-W.Y.), qianwang.jhmi@gmail.com (Q.W.). Editorial Correspondence: Dr. King-Wai Yau, Johns Hopkins University School of Medicine, PCTB 905A, 725 North Wolfe Street, Baltimore, MD 21205, Tel: 410-955-1260, Fax: 410-955-1948, kwyau@jhmi.edu.

†Present Address: Department of Biology, Stanford University, Stanford, CA 94305, USA

+Present Address: Department of Physiology, University of California San Francisco, San Francisco, CA 94158, USA

^Present Address: Center for Neural Repair and Rehabilitation, Temple University School of Medicine, Philadelphia, PA 19122, USA

AUTHOR CONTRIBUTIONS

Q.W., Z.J., T.X., and K.-W.Y. designed the experiments on the isolated mouse iris. Q.W. carried out all muscle recordings (with important initial help from T.X.), immunostaining of mouse iris, qRT-PCR experiments, generated and characterized the *Opn4*$^{f/f}$ mouse line. W.W.S.Y. generated the *Opn4-Cre* line with help from S.H.K. in D.E.B’s laboratory. Z.J. bred the *Opn4-Cre;Gα11*$^{-/-}$*Gαq*$^{f/f}$, and *Opn4-Cre;Gα11*$^{-/-}$*Gαq*$^{f/f}$*;Gα14*$^{-/-}$ mouse lines required for experiments. K.M. provided the IP3R gene-knockout lines, and S.O. provided the *Gαq*$^{f/f}$*;Gα11*$^{-/-}$ line. Q.W., W.W.S.Y. and K.-W.Y. wrote the paper.

Competing financial interests: The authors declare no competing financial interests.

muscle itself may express melanopsin [5], or its cholinergic parasympathetic innervation may be modulated by suggested intraocular axonal collaterals of ipRGCs traveling to the eye's ciliary body or even to the iris [20–22]. Here, we show that the muscarinic receptor antagonist, atropine, eliminated the effect of acetylcholine (ACh), but not of light, on isolated mouse sphincter muscle. Conversely, selective genetic deletion of melanopsin in smooth muscle mostly removed the light-induced but not the ACh-triggered increase in isolated sphincter muscle's tension, and largely suppressed the local PLR *in vivo*. Thus, sphincter muscle cells are *bona fide*, albeit unconventional, photoreceptors. We found melanopsin expression in a small subset of mouse iris sphincter muscle cells, with the light-induced contractile signal apparently spreading through gap junctions into neighboring muscle cells. Light and ACh share a common signaling pathway in sphincter muscle. In summary, our experiments have provided details of a photosignaling process in the eye occurring entirely outside the retina.

In Brief

Wang et al. show that a subset of mouse iris sphincter muscle cells express the visual pigment, melanopsin, with its photoactivation leading to muscle contraction and pupillary constriction. Thus, mouse iris sphincter muscle cells are *bona fide*, albeit unconventional, photoreceptors.

RESULTS

ACh- and Light-Induced Tension in Isolated Mouse Iris Sphincter Muscle

We mounted an isolated mouse sphincter muscle between a stationary anchor and a micronewton (μN)-strain gauge for isometric-tension measurements, stretched optimally to give the largest light response under continuous perfusion at 36–37ºC ([5]; STAR METHODS). An ACh step elicited a robust tension increase in the wild-type (WT) mouse muscle with little adaptation over many seconds (Figure 1A, left) [5]. The averaged data gave a dose-response relation with maximum tension of 305.0 ± 50.5 μN (mean ± SD, 6 muscles) and a half-saturating ACh concentration of 18.7 μM (Figure 1A, right). A light flash also increased muscle tension [5], typically with a fast peak followed by a slower second peak for a moderate-to-intense flash (Figure 1B, left). The extrapolated maximal force at initial peak was 88.4 ± 11.1 μN (6 muscles) (Figure 1B, right), considerably smaller than the ACh response; this is true even for a light step (Figure 1B inset). The averaged data gave a flash intensity-response relation with a half-saturating flash intensity of 1.8×10^9 photons μm^{-2} at 436 nm (Figure 1B right), ~50-fold higher in equivalent 480-nm light than for mouse M1 ipRGCs [23]. The response's second peak likely reflected a tension rise coming from neighboring muscle cells due presumably to Ca^{2+} spreading through gap junctions between iris sphincter muscle cells [24–26]. Indeed, the second peak was inhibited reversibly by the gap-junction blockers, 500-μM octanol or 200-μM carbenoxolone (CBX) (Figure 1C). Because these blockers also affect voltage-gated Ca-channels [27], the additional involvement of the latter in this spread cannot be ruled out. The large difference in maximal increase in tension between ACh- and light-stimulations appears to result from the low percentage of sphincter muscle cells expressing melanopsin compared to practically all cells expressing muscarinic receptors (see later). A photosensitive muscle cell may also have abundant muscarinic receptors versus a low melanopsin density.

In the steady presence of a low ACh concentration (100-μM), light elicited in the sphincter muscle an inexplicable rapid transient decrease in tension followed by an increase beyond the ACh-induced baseline tension (Figure S1A). As background ACh concentration increased, so did the steady tension; concomitantly, the light-induced incremental tension progressively decreased (Figure S1A; 400-μM ACh) or literally disappeared (Figure S1B; 1-mM ACh). The mechanistic convergence of light and ACh signals in the muscle is analyzed below.

Independence of Light-Induced Muscle Tension on Cholinergic Transmission

We next asked whether ipRGCs' collateral axonal processes – if indeed present in the iris/iris periphery [20–22] – underlie the sphincter muscle's local light response, possibly by presynaptically activating the parasympathetic cholinergic terminals innervating the muscle [20,21]. We found no effect of 1-μM tetrodotoxin (TTX, bath-applied for 1 hr to block axonal spike activity) on the muscle's flash response (Figure 2A). More importantly, we found also no effect on the light response after blocking muscarinic transmission from parasympathetic innervation to sphincter muscle with bath-applied 10-μM atropine, even though this manipulation eliminated the muscle's ACh response (Figure 2B top and bottom). Finally, knocking out M_1 and M_3 muscarinic receptors on the sphincter muscle [28–31] (*Chrm1*$^{-/-}$;*Chrm3*$^{-/-}$ genotype) removed the ACh response but spared the light response (Figure S2A, $P > 0.05$ versus $P < 0.01$, unpaired two-sample *t*-test). Thus, any ipRGC axonal collaterals in the iris, even if existent, do not convey light signals to activate sphincter-muscle contraction through modulating muscarinic transmission.

IpRGCs contain glutamate and pituitary adenylate cyclase-activating peptide (PACAP) [32,33]. Although vertebrate muscle is not known to have glutamate receptors, we checked this out nonetheless, but found no effect of bath-applied inhibitors for ionotropic and metabotropic glutamate receptors (STAR METHODS) on the muscle's light response, nor any increase in dark muscle tension produced by bath-applied glutamate (1-mM) with or without 100-μM cyclothiazide (inhibitor of AMPA-receptor desensitization) (Figure S2B). 100-nM PACAP 6–38 (PACAP-receptor antagonist) also did not reduce the light response, nor did 100-nM PACAP 1–27 and 1–38 (PACAP-receptor agonists) increase dark muscle tension (Figure S2C). These results suggest that the photosensitivity of mouse iris sphincter muscle cells is also unlikely to come from direct ipRGC innervation of the muscle even if ipRGC processes are present.

Smooth-Muscle-Specific Ablation of Melanopsin Drastically Reduces Sphincter-Muscle Photosensitivity

To determine whether melanopsin indeed is present and also signals in the iris sphincter muscle, we took a functional approach by genetically ablating melanopsin selectively in smooth muscle (to which the iris sphincter muscle belongs). We crossed a smooth-muscle-Cre line (*smMHC-Cre*; [34]) to an *Opn4*$^{f/f}$ line (Figure S3A; STAR METHODS) to obtain *smMHC-Cre;Opn4*$^{f/f}$ progenies. From quantitative RT-PCR, the level of *Opn4* mRNA in the iris sphincter of these mice was only 10% of WT, versus a still-normal level in these animals' retina, thus confirming muscle specificity (Figure 2C, $P < 0.01$ versus $P > 0.05$, unpaired two-sample *t*-test). Immunolabeling of melanopsin-expressing ipRGCs in

the *smMHC-Cre;Opn4*$^{f/f}$ retina also remained normal (Figure S3B). In this genotype, the transient peak of the muscle's flash-induced tension near the saturating flash intensity was drastically reduced (by about 85%) from WT, although the ACh response stayed essentially normal (Figure 2D, top and bottom, $P < 0.01$ versus $P > 0.05$, unpaired two-sample t-test). The small residual light response in *smMHC-Cre;Opn4*$^{f/f}$ muscle possibly came from an incomplete removal of melanopsin by the Cre-Lox system. These observations support the functional presence of melanopsin in sphincter muscle normally.

We also performed whole-animal PLR with this smooth-muscle-specific melanopsin-knockout line. Figure 2E left shows the overall *in vivo* PLR in both eyes of WT mice when step-illuminated on one eye [5]. Only PLR behavior at intermediate light intensities is shown here (see [5] for the full intensity range). The WT peak fractional pupil constriction (in area) was stronger ipsilaterally than contralaterally [5], with the difference shown in Figure 2F. This bilaterally asymmetrical overall PLR, most evident at $<10^{-9}$-10^{-7} μJ μm^{-2} s^{-1} (505 nm) [5], arises from the melanopsin-mediated local PLR and from any intrinsic bilateral asymmetry in effectiveness of the brain's PLR circuitry [5]. This asymmetry in *smMHC-Cre;Opn4*$^{f/f}$ mice (Figure 2E middle and 2F) was much less than that in WT (Figure 2E middle and 2F), due to loss of melanopsin in sphincter muscle (we did not observe melanopsin in dilator muscle; see later). The asymmetry in *Opn4*$^{KOF/KOF}$ (equivalent to unconditional *Opn4*$^{-/-}$; Figure S3A and STAR METHODS) was also much reduced from WT, in fact approaching zero (Figure 2E right and 2F), which implies negligible asymmetry in effectiveness of the brain's PLR circuitry at least for these particular animals. The small residual difference between *smMHC-Cre;Opn4*$^{f/f}$ and *Opn4*$^{KOF/KOF}$, if real, may reflect slightly incomplete Cre activity. In summary, melanopsin's contribution to the local PLR originated predominantly from its presence in the muscle.

Melanopsin Expression in Mouse Iris

Here, we sought to visualize melanopsin in the iris. Quantitative RT-PCR confirmed melanopsin transcripts in mouse iris (Figure S3C), as we found previously [5]. Despite a higher melanopsin-immunoreactivity in the sphincter-muscle region, we found no distinctly labeled muscle cells or axon-like structures in the whole-mount mouse iris, possibly due to a low melanopsin protein level as in M4- and M5-ipRGCs [12,35]. As an alternative approach, we used X-gal labeling of the *Opn4*$^{\tau lacZ/+}$ iris [11] in an albino background (see STAR METHODS) to facilitate detection. Despite strong labeling in the retina, we found no obvious signal in the iris (Figure S4A). Earlier, with *Opn4-tdTomato* BAC transgenic mice, we did detect weak tdTomato fluorescence in the iridic sphincter region next to the pupil [5]. To enhance the melanopsin signal, we generated an *Opn4-Cre* BAC transgenic mouse (STAR METHODS) and bred it to *Rosa-tdTomato* (*Ai9*) [36] or *Rosa-Alkaline Phosphatase* (*R26iAP*) [37] reporter lines. The *Opn4-Cre;Ai9* genotype correctly labeled retinal ipRGCs (Figure 3A), including some with no obvious melanopsin immunosignal (M4- and M5-subtypes) and vice versa [12,35]. In each albino *Opn4-Cre;R26iAP* iris, we found ~30 labeled muscle cells in several clusters around the pupil (Figure 3B). These labeled cells represented only a small percentage (~10% or less) of all sphincter muscle cells (assuming similar total numbers of sphincter muscle cells in mouse and rat; [38]). Similar labeling was observed in the albino *Opn4-Cre;Ai9* iris, which showed melanopsin

co-localization with α-smooth muscle actin (αSMA, a smooth-muscle marker) (Figure 3C) and M_3 muscarinic receptor (Figure 3D). Practically all sphincter muscle cells expressed M_3 muscarinic receptor (Figure 3E). Thus, most if not all sphincter muscle cells can respond to ACh released by parasympathetic nerve terminals, but only a small percentage are intrinsically photosensitive, consistent with the much smaller muscle tension triggered by light than by ACh (see Figure 1A, B).

Genetic labeling also detected sporadic *Opn4-Cre* activity in the iris dilator region (Figure 3B and S4B,C) – not in the muscle layer but in cells more posterior (Figure S4B and legend). Colocalization of this signal with PAX6 (Figure S4C), a transcription factor present in all adult iris smooth muscle cells and iris pigmented epithelial (IPE) cells [39,40], suggests these labeled cells likely being IPE cells (with phagocytic function in culture; [41]). Occasionally, such cells were found in the sphincter region (Figure 3B, left). This labeling in adult tissue may be genuine, or may reflect merely transient *Opn4*-promoter activity during development.

Consistent with earlier reports [22,42], we observed a plexus of melanopsin-immunolabeled processes at the edge of the mouse retina (Figure S4D), but did not detect their invasion anywhere into the ciliary body or iris as reported [21,22].

Mechanism of Melanopsin-Signaling and Convergence with ACh Signaling in Sphincter Muscle

We previously found that the mouse iris sphincter muscle, like M1-ipRGCs, requires phospholipase C-β4 (PLCβ4) for photosignaling [5]. To further examine phototransduction in this muscle, we started with the mediating G-protein by focusing on the $G\alpha_q$-subfamily members: $G\alpha_q$, $G\alpha_{11}$, $G\alpha_{14}$, and $G\alpha_{15}$ [43–45]. We found that the peak flash-induced tension increase was reduced by up to 80% at the highest flash intensity tested in *Opn4-Cre;*$Ga_q^{f/f}$*;*$Ga_{11}^{-/-}$ double-KO and *Opn4-Cre;*$Ga_q^{f/f}$*;*$Ga_{11}^{-/-}$*;*$Ga_{14}^{-/-}$ triple-KO muscles, but was not affected in *Opn4-Cre;*$Ga_q^{f/f}$ single-KO, $Ga_{11}^{-/-}$*;*$Ga_{14}^{-/-}$ double-KO, and $Ga_{15}^{-/-}$ single-KO muscles (Figure 4A upper, left and middle). These findings suggest a functional redundancy between Ga_q and Ga_{11}, which is generally not unusual [43–45]. In *Opn4-Cre;*$Ga_q^{f/f}$*;*$Ga_{11}^{-/-}$ double-KO, the large reduction in muscle response contrasted with the merely mildly reduced retinal ipRGC light response [46,47]. As knocking out Ga_{14} additionally (i.e., *Opn4-Cre;*$Ga_q^{f/f}$*;*$Ga_{11}^{-/-}$*;*$Ga_{14}^{-/-}$ triple-KO) did not further reduce the muscle response, Ga_{14} apparently has a small or negligible role. The incomplete removal of the light response in *Opn4-Cre;*$Ga_q^{f/f}$*;*$Ga_{11}^{-/-}$*;*$Ga_{14}^{-/-}$ may indicate that the *Opn4* promoter (relatively weak in our experience) is not strong enough for producing sufficient Cre to ablate Ga_q in all melanopsin-positive cells. Alternatively, $G\alpha_{15}$ may underlie the small residual response, with the normalcy of $Ga_{15}^{-/-}$ explainable by redundancy (Figure 4A upper, left and middle). The Ga_{15} and Ga_{11} genes are tightly linked, thus ruling out making a quadruple-KO mouse. The ACh responses of the above *Opn4-Cre*-driven KOs were only moderately smaller than WT (Figure 4A upper, right). This is not surprising because *Opn4-Cre* affects only the melanopsin cells; thus, the great majority of muscle cells still express $G\alpha_q$. In short, melanopsin and muscarinic-receptor signalings converge largely at $G\alpha_q$/$G\alpha_{11}$, with $G\alpha_{14}$ or $G\alpha_{15}$ potentially also having a small role.

We also checked the other PLCβ isoforms besides PLCβ4, namely, PLCβ1–3. Surprisingly, *Plcβ2*$^{-/-}$ muscles, like *Plcβ4*$^{-/-}$, showed a severely defective light response (Figure 4A bottom, left and middle). Unfortunately, non-viable *Plcβ2*$^{-/-}$;*Plcβ4*$^{-/-}$ double-KO and difficulty in producing double-KO progenies for the other PLCβ subunits ruled out further study. For the ACh response, *Plcβ1*$^{-/-}$ showed no effect, while *Plcβ2*$^{-/-}$, *Plcβ3*$^{-/-}$ and *Plcβ4*$^{-/-}$ single-KOs all gave responses only moderately smaller than WT (Figure 4A bottom, right). The simplest interpretation is that the melanopsin-expressing muscle cells express a more restrictive set of PLC isoforms (PLCβ2 and PLCβ4) than do non-melanopsin-expressing muscle cells (PLCβ2, PLCβ3 and PLCβ4), which are the majority, thus rendering a higher PLCβ-isoform redundancy in ACh signaling. Alternatively, melanopsin and ACh signalings may be segregated differentially at the subcellular level with respect to the PLCβ isoforms.

Finally, in smooth muscle, the inositol 1,4,5-trisphosphate receptor (IP_3R) interposes between the second messenger, IP_3, produced by PLCβ and the intracellular release of Ca^{2+}, which ultimately triggers muscle contraction [48]. Of the three known IP_3R types (IP_3R1 to 3), IP_3R1 is ubiquitously expressed in various tissues including smooth muscle [49,50]. Indeed, *Itpr1*$^{-/-}$ muscle exhibited little response to light and ACh (Figure 4B, left and right), whereas the *Itpr2*$^{-/-}$;*Itpr3*$^{-/-}$ double-KO responded normally to light (Figure 4B, middle) and ACh (not shown).

In short, melanopsin in the iris sphincter muscle signals primarily through $G\alpha_{q/}G\alpha_{11,}$ PLCβ2/ PLCβ4, and IP_3R1 to elicit a rise in Ca^{2+} and muscle contraction. ACh signals largely similarly.

DISCUSSION

We conclude in this work that the local PLR originates predominantly, if not exclusively, from melanopsin in the sphincter muscle itself. The local-PLR phenomenon may be general to nocturnal and crepuscular sub-primate mammals, although absent in diurnal sub-primates and nocturnal/diurnal primates [5]. We found no evidence for the suggestion by others of a melanopsin-mediated light signal going sequentially through intraocular ipRGC axonal collaterals, then parasympathetic presynaptic terminals, and eventually to the sphincter muscle via muscarinic synaptic transmission [20,21].

Our functional experiments have focused on the isolated sphincter muscle, partly prompted by others' reports [20,21] and partly to avoid complexities associated with the intact eye [4,21,22] or the isolated anterior chamber [3,4,22,51] being the experimental preparation, in which the pupil size is controlled by the antagonistic sphincter and dilator muscles. The intact eye's enclosed geometry also makes pharmacological results difficult to interpret owing to uncertainties regarding drug penetration and site-specificity or completeness of drug action, presumably the reason why there are some inconsistencies across investigators [4,21,22]. The isolated sphincter muscle overcomes these challenges. We cannot completely exclude some yet-unknown modulation of the dilator muscle by ipRGCs that contribute to the local PLR as well. However, given the greatly diminished bilateral asymmetry in overall PLR under monocular illumination in *smMHC-Cre;Opn4*$^{f/f}$ compared to WT mice (Figure

2F), together with the genetic-labeling experiments (Figure 3B and S4B), any melanopsin signaling in the iris other than that being intrinsic to the sphincter muscle is likely minor.

As for the co-existent melanopsin-signaling and ACh-signaling in the small subset of intrinsically-photosensitive sphincter muscle cells, the two appear to converge at the G-protein level (see RESULTS). Presumably, this sharing in mechanism allows the brain-driven PLR and the local PLR to be concurrently modulatable. Furthermore, the existence of gap junctions between adjacent sphincter muscle cells allows the contraction from the sparse melanopsin-expressing cells to spread more evenly across the sphincter, hence more uniform constriction of the pupil.

Interestingly, there appears to be an evolutionary trend toward disappearance of the local PLR. In the primitive jawless fish (cyclostomes) such as lamprey, there is supposedly no central PLR other than a local PLR involving an intrinsically-photosensitive sphincter muscle [6]. In amphibians, the local PLR still dominates although neural innervation has come to exist [6,7]. Among nocturnal and crepuscular sub-primate mammals [5], such as mouse, the local PLR persists but already appears to be of secondary importance, with the duplicity of PLR (i.e., local and central) leaning more toward central control. In diurnal sub-primates as well as nocturnal and diurnal primates, we found the local PLR to be absent [5]. Viewed in this context of evolutionary-developmental biology, our confirmation of the local mouse iridic photosensitivity residing in the sphincter muscle itself therefore seems to be reasonable. In this context, it may also be relevant to note that the mammalian iris sphincter muscle (and dilator muscle) happens to be a rare case of ectoderm- rather than mesoderm-derived muscle [39] long thought to originate from the same stem cells as do photoreceptors [6]. The reason for the local PLR's disappearance in primates and diurnal sub-primates nonetheless remains rather unclear.

STAR METHODS

CONTACT FOR REAGENT AND RESOURCE SHARING

Further information and requests for resources and reagents should be directed to the Lead Contact, King-Wai Yau (kwyau@jhmi.edu).

EXPERIMENTAL MODEL AND SUBJECT DETAILS

Mice—All procedures involving mice were approved by the Johns Hopkins University School of Medicine Institutional Animal Care and Use Committee. Genetically-engineered mouse lines used in this study included *Opn4*$^{\tau lacZ/\tau lacZ}$ [11], *Chrm1*$^{-/-}$;*Chrm3*$^{-/-}$ [52,53], *Gα*$_q^{f/f}$ [54], *Gα*$_{11}^{-/-}$ [55], *Gα*$_{14}^{-/-}$ [56], *Gα*$_{15}^{-/-}$ [56], *Plcβ1*$^{-/-}$ [57], *Plcβ2*$^{-/-}$ [58], *Plcβ3*$^{-/-}$ [59], *Plcβ4*$^{-/-}$ [60], *Itpr1*$^{-/-}$ [61], *Itpr2*$^{-/-}$;*Itpr3*$^{-/-}$ [62], *smMHC-Cre* [34];*Opn4*$^{f/f}$ (see below), *Opn4*$^{KOF/KOF}$ (see below), *Opn4-Cre* (see below), *Ai9*, and *R26iAP* (The Jackson Laboratory). C57BL/6J (genetic background for many of the above lines; The Jackson Laboratory) was used as WT controls for most experiments. C57BL/6J-Tyr^{c-2J}/J mice (The Jackson Laboratory), an albino strain, were used as WT controls for experiments involving *Chrm1*$^{-/-}$;*Chrm3*$^{-/-}$ mice (which are in albino background). To obtain reproducible force measurement, we typically used animals with age of 3 months

± 5 days. For *Plcβ1*$^{-/-}$, only one 2-year-old animal (Figure 4A bottom, middle) was used owing to the very limited homozygous animals available. *Itpr1*$^{-/-}$ homozygous animals die before postnatal day 25–28, so we used P23 mice for experiments, with age-matched WT as control. For Figure 3 and Figure S4, an albino background (see above) was used to help visualize fluorescent reporters in mouse iris.

Generation of *smMHC-Cre;Opn4*$^{f/f}$ line—Targeted C57BL/6N embryonic stem cells were obtained from UCDAVIS KOMP repository (clone EPD0642_3_D12), and subsequently injected into the B6(Cg)-*Tyr*$^{c-2J}$/J blastocysts at the Transgenic Core Facility of Johns Hopkins University School of Medicine. The mice generated from successful germline transmission were heterozygous for the "knock-out first" allele (i.e. *Opn4*$^{KOF/+}$; see Figure S3A). Exposure of the construct to flippase [by breeding with ACTB:FLPe B6J mouse line (The Jackson Laboratory)] resulted in removal of the trapping cassette and expression of the *Opn4* gene. The second exon of *Opn4* remained floxed, but was later removed conditionally after breeding to the *smMHC-Cre* mouse line [34], resulting in a loss-of-function allele in smooth muscle cells. *smMHC-Cre*-positive male mice were chosen for breeding in order to avoid germ-line recombination of the maternal *floxed-Opn4* allele, and to reduce obstructed labour associated with the expression of the *smMHC-Cre* transgene in the uterus. Genotyping primers for the floxed alleles are as follows: Floxed-Opn4 (PostFlp) forward: 5'-TCT ACA CAG TGG CTG AGA CAA GAG G-3', Floxed-Opn4 (PostFlp) reverse: 5'- AAG AGG GAG TGA AAG GCT CAG ATG G-3' (product 710bp in size); WT primers are the same as the primers for genotyping the floxed allele, except that the product is 554 bp in size.

Generation of *Opn4-Cre* line—The Cre recombinase cDNA, followed by the rabbit β-globin poly-A signal, were inserted immediately after the start codon in exon 1 of the mouse *Opn4* gene in a bacterial artificial chromosome (BAC) clone (BACPAC Resource Center, RP23–340N18) by bacterial homologous recombination. Successful modifications were confirmed by PCR and Southern blot. The modified BAC was linearized by enzyme digestion with AscI and SrfI, and subsequently injected into the pronuclei of B6SJLF2 embryos at the Transgenic Core Facility of Johns Hopkins University School of Medicine. Three transgenic founders were identified by PCR on genomic DNA (Forward primer: 5'-TGT GAA GGA CAG AGC CTC CT −3'; Reverse primer: 5'- CAG CCC GGA CCG ACG ATG AAG −3') and were bred with wildtype C57BL/6J mice to establish transgenic lines. One of these lines showed specific expression of tdTomato in ipRGCs when crossed to *Rosa-tdTomato* line – 85% of melanopsin-immunopositive cells were tdTomato-labeled and 91% of cells showing tdTomato fluorescence were immunopositive for melanopsin (altogether 2,342 cells from 3 animals analyzed). Some of the tdTomato-positive, OPN4-immunonegative cells may be M4 or M5 ipRGCs, which were reportedly not stained by melanopsin antibody (AB-N38, Advanced Targeting Systems) under regular conditions [12]. Electrophysiologically, every RGC labeled by *Opn4-Cre*-driven reporters and tested so far was intrinsically photosensitive (>150 cells). In the sphincter muscle, some labeled muscle cells could be individually identified. For those in a small cluster, we made our best effort to estimate the approximate number of muscle cells therein, facilitated by the average length of solitary labeled cells (344 ± 58 μm, mean ± SD, n = 8).

METHOD DETAILS

Iris-sphincter-muscle force measurement—An isolated iris sphincter muscle with anterior- and posterior-associated connective tissue was prepared as previously described [5]. Briefly, under infrared illumination, the anterior chamber of a mouse eye enucleated from an overnight-dark-adapted animal was first excised by a circumferential cut along the ciliary body. The dilator muscle was subsequently trimmed away with a razor blade. Next, the iris sphincter muscle was separated from the cornea, transferred into a recording chamber superfused with Ames medium (equilibrated with 95%O_2/5%CO_2) at 36–37 ºC at a flow rate of 3 ml/min. Under infrared light, the muscle ring was mounted horizontally on an upright microscope between two stainless-steel hooks attached to micromanipulators. One hook was fixed and the other attached to a force sensor (see below). The muscle ring was slowly stretched to a length of 1.0–1.2 mm for 3-month old mice, found to give roughly maximum light-induced force.

Muscle force was measured with a fabricated device broadly as published [5]. The device contains a single-crystal silicon strain-gauge with μ-Newton sensitivity (AE-801, Sensor One), with signals being amplified by a custom circuitry. The force sensor was coated with a suspension of carbon powder in silicone in order to protect it from light and moisture. The voltage output of the sensor was proportional to the applied force (187-μN/V, calibrated by hanging various pre-measured weights fabricated from a thin silver wire), with a non-linearity of <0.1%. The signal was digitized by Digidata 1440A and acquired by pClamp 10.0. For light responses, the muscle contraction was induced by flashes (10–300 msec), with intensity and duration being proportionally interchangeable without affecting the response. We used a flash instead of a light-step for stimulation because the muscle did not readily recover from a light-step even of moderate intensity. Hg-light was used in conjunction with a 436 nm interference filter. Light was delivered through a 5× objective as a uniform spot of 5-mm diameter on the muscle, large enough to cover the entire preparation for mouse. White light was used for saturating the response owing to the limited monochromatic light intensity available. White flashes were converted to equivalent 436-nm or 480-nm flashes by response-matching in the linear range. The light response of the mouse iris recovered quite slowly, so we separated light-stimulation trials by ≥10 min intervals.

ACh was bath-applied and controlled by solenoid valves. We did not examine brief ACh pulses because the muscle's relatively large size and thickness created difficulty in administering brief, temporally well-defined ACh pulses across the entire muscle. After a period of baseline recording, the Ames medium was switched to ACh at different concentrations in Ames. Once the steady response was reached, the ACh was immediately switched off and control Ames switched on to wash out the ACh. Pharmacological reagents were likewise bath-applied.

***In situ* pupillometry—**All animals were kept in 12 hr/12 hr light/dark cycle before experiments. The experiments were performed between 2 hours after lights-on and 2 hours before lights-off with >1-hr dark adaptation. To simultaneously monitor the PLR in both eyes, we hand held the animals and used a pupillometer with LED light (505 nm) for stimulation via a Ganzfeld sphere as previously described [5]. The fractional constriction of

the pupil at peak in Figure 2E is defined as $(A_{dark} - A_{light})/A_{dark}$, where A_{dark} and A_{light} are the pupil areas in darkness and in steady light, respectively. The PLR is relatively slow; we took measurement when it reached a peak value, hence the word “peak” in Figure 2E.

Solutions—For iris-sphincter-muscle force measurements, the bath solution was bicarbonate-buffered Ames medium (Sigma). Cholinergic synaptic transmission was blocked by 10-μM atropine (Sigma). Glutamatergic synaptic transmission was blocked by 20-μM DNQX for AMPA and kainite receptors, 50-μM DL-2-amino-5-phosphonopentanoic acid for NMDA receptors, and 250-μM DL-2-amino-4-phosphonobutyric acid for metabotropic glutamate receptors (all Sigma). We applied 1-μM tetrodotoxin (Alomone Labs) to muscles to block action potentials in any residual ipRGC axonal terminals (if they exist as reported). To test whether any contraction could be elicited by glutamatergic and PACAP agonists, we used 1-mM L-glutamic acid (Sigma), 100-nM-PACAP 1–27 and 1–38 (Tocris, UK). To reduce the desensitization effect of metabotropic glutamatergic receptors, 100-μM cyclothiazide (Tocris) was applied together with glutamate. PACAP 6–38 (100-nM, Tocris) was used as an antagonist for PACAP receptors. Two broad-spectrum gap junctional blockers, octanol (500-μM) and carbenoxolone (200-μM) (both Sigma) were used for testing the role of gap junctions in the light-induced contraction of the isolated iris sphincter muscle.

Immunohistochemistry and other procedures—Mice were anesthetized by intraperitoneal injection of ketamine (100-mg/kg body weight) and xylazine (5-mg/kg body weight), and were perfused with phosphate buffered saline (PBS) followed by 4% paraformaldehyde (PFA) in PBS. For immunohistochemistry on flat-mount retinas or whole-mount irises, the eyes were enucleated from the perfused, with irises and retinas isolated and fixed for 30 min at room temperature in 4% PFA. After initial washes with PBS containing 0.5% Triton X-100 (i.e., PBST), tissues were blocked with 1% tyramide blocking solution (Life Technologies) in PBST overnight at 4°C. The tissues were then incubated with primary antibody in the same blocking solution overnight at 4°C. The primary antibodies used in this study included a polyclonal antibody against mouse melanopsin (AB-N38, which recognizes the first 15 amino acids at the N-terminus in both OPN4L and OPN4S, Advanced Targeting Systems, 1:2500 dilution), a polyclonal antibody against α-smooth muscle actin (ab21027, AbCam, 1:150 dilution), a polyclonal antibody against M3 muscarinic receptor (AS3741S, Research and Diagnostics Antibodies, 1:250 dilution), a polyclonal antibody against PAX6 (PRB-278P, Covance, 1:500 dilution). After washing, the tissues were exposed to secondary antibodies at 1:500 dilution for 3 hr at room temperature. Tissues were mounted with anti-fade reagent containing 4’, 6’-diamidino-2-phenylindole (DAPI) and cover-slipped. Images were captured on a Zeiss LSM 510 confocal microscope.

For X-gal staining, freshly-dissected mouse iris and retina were fixed in 0.2% glutaraldehyde in 0.1-M phosphate buffer containing 2-mM $MgCl_2$ and 5-mM EGTA for 15 min. The tissues were then washed in 0.1-M phosphate buffer containing 2-mM $MgCl_2$, 0.01% sodium deoxycholate and 0.02% Nonidet P-40 for three times. Staining was carried out at 37 °C (overnight) in a solution of the above buffer containing X-gal at a final concentration of 1-mg/ml, 5-mM $K_3Fe(CN)_6$, and 5-mM $K_4Fe(CN)_6$.

For alkaline phosphatase staining, freshly-dissected tissue was fixed in 0.2% glutaraldehyde in 0.1-M Tris-HCl. The endogenous alkaline phosphatase activity was heat-inactivated at 65 °C for 30 min. Staining was carried by using Vector® Blue Substrate kit (Vector labs) following manufacturer's instructions.

Quantitative RT-PCR—Total RNA was extracted from mouse tissues using the TRIzol Reagent (Invitrogen) according to the manufacturer's instructions. First-strand cDNA was synthesized from 2-μg DNase-treated total RNA using an oligo-dT primers and SuperScript® III reverse transcriptase (Invitrogen). Quantitative-PCR amplification and analysis were carried out with SYBR Green PCR Master Mix (Applied Biosystems) in an Applied Biosystems 7500 Real-Time PCR System by using the following primer sets: *Opn4S* (5'-GCT ACC GCT CTA CCC ACC −3' and 5'- CTA CAT CCC GAG ATC CAG ACT G-3'), *Opn4L* (5'- GCT ACC GCT CTA CCC ACC −3' and 5'- CAC CTT GGG AGT CTT AGA TCT CTG −3') and *β-actin* (5'- AAA GAG AAG CTG TGC TAT GTT G −3' and 5'- CAT AGA GGT CTT TAC GGA TGT C −3'). Primers for detecting the WT *Opn4* allele in the *smMHC-Cre;Opn4*$^{f/f}$ genotype are: Opn4E1–2F (5'-TAG CCC CAC GAC ATC TGC A-3') and Opn4E-3R (5'- GTA GAG GCT GCT GGC AAA GA −3'). The specificity of the SYBR green PCR signal was further confirmed by melting-curve analysis and agarose gel electrophoresis. To estimate the relative abundance of the mouse *Opn4* short and long isoforms, *Opn4S* and *Opn4L*, standard DNA templates were generated by ligating the respective amplicon into the pGEM®-T Easy Vector (Promega). Standard curves were generated by plotting the threshold cycle (C_T) against the log copy number of the standard DNA templates. The absolute copy number for *Opn4S* or *Opn4L* in each sample was calculated based on the standard curves, which were further divided by the absolute copy number of *β-actin* in the same sample. In Figure 2C, the abundance of total *Opn4* in iris sphincter or retina from WT, *smMHC-Cre;Opn4*$^{f/f}$ and *Opn4*$^{KOF/KOF}$ mice was normalized to that in the WT iris sphincter. In Figure S3C, the abundance of individual isoforms of *Opn4* in iris or retina was normalized to that of *Opn4L* in the retina.

QUANTIFICATION AND STATISTICAL ANALYSIS

The definition of statistical parameters and the exact values of n (number of muscles or animals, depending on the types of experiments) were reported in the corresponding figure legends. Most data were presented as mean ± SD. Statistical analyses (paired or unpaired two sample *t*-test) were performed using Excel.

Supplementary Material

Refer to Web version on PubMed Central for supplementary material.

ACKNOWLEDGEMENTS

We thank the following individuals for providing knockout mouse lines: J. Wess (NIH-NIDDK, *Chrm1*$^{-/-}$;*Chrm3*$^{-/-}$), J. Nathans (Johns Hopkins School of Medicine, *R29iAP*), H.-S. Shin (Korea Institute of Science and Technology, *Plcβ1*$^{-/-}$), N. Ryba (NIH/NIDCR, *Plcβ2*$^{-/-}$), M. Simon (University of California, San Diego, *Gα14*$^{-/-}$, *Plcβ3*$^{-/-}$, and *Plcβ4*$^{-/-}$), T. Wilkie (University of Texas Southwestern Medical Center, *Gα15*$^{-/-}$). We thank M. Ma (University of Pennsylvania) and J. Wess (NIH-NIDDK) for providing antibodies against M_3 muscarinic receptor for us to try. We thank T. Shelley for fabricating all custom equipment, X. Ren for help on western blot, and L. Ding for mouse-genotyping support. Members of the Yau laboratory (Y. Sheng, D.

Silverman, X. Ren, R. Li and L. Chen) provided comments on the manuscript. This work was supported by NIH Grant EY014596 and the António Champalimaud Vision Award, Portugal to K.-W.Y., NINDS Core Center Grant P30 NS050274, and a HHMI International Predoctoral Fellowship to W.W.S.Y. T.X. was supported by National Key Basic Research Program of China (2013CB967700, 2016YFA0400900), National Natural Science Foundation of China (31322024, 81371066, 91432104) and Strategic Priority Research Program of the Chinese Academy of Science (XDB02010000).

REFERENCES

1. Oyster CW (1999). The Human Eye: Structure and Function (Sinauer Associates)
2. McDougal DH, and Gamlin PD (2015). Autonomic control of the eye. Compr. Physiol 5, 439–473. [PubMed: 25589275]
3. Bito LZ, and Turansky DG (1975). Photoactivation of pupillary constriction in the isolated in vitro iris of a mammal (Mesocricetus auratus). Comp. Biochem. Physiol. -- Part A Physiol 50, 407–413.
4. Lau KC, So KF, Campbell G, and Lieberman AR (1992). Pupillary constriction in response to light in rodents, which does not depend on central neural pathways. J. Neurol. Sci 113, 70–79. [PubMed: 1469457]
5. Xue T, Do MT, Riccio A, Jiang Z, Hsieh J, Wang HC, Merbs SL, Welsbie DS, Yoshioka T, Weissgerber P, et al. (2011). Melanopsin signalling in mammalian iris and retina. Nature 479, 67–73. [PubMed: 22051675]
6. Barr L (1989). Photomechanical coupling in the vertebrate sphincter pupillae. Crit. Rev. Neurobiol 4, 325–366. [PubMed: 2655940]
7. Barr L, and Alpern M (1963). Photosensitivity of the Frog Iris. J. Gen. Physiol 46, 1249–1265. [PubMed: 14043001]
8. Kargacin GJ, and Detwiler PB (1985). Light-evoked contraction of the photosensitive iris of the frog. J. Neurosci 5, 3081–3087. [PubMed: 3932607]
9. Seliger HH (1962). Direct action of light in naturally pigmented muscle fibers. I. Action spectrum for contraction in eel iris sphincter. J. Gen. Physiol 46, 333–342. [PubMed: 13992712]
10. Tu DC, Batten ML, Palczewski K, and Van Gelder RN (2004). Nonvisual photoreception in the chick iris. Science 306, 129–131. [PubMed: 15459395]
11. Hattar S, Liao HW, Takao M, Berson DM, and Yau KW (2002). Melanopsin-containing retinal ganglion cells: architecture, projections, and intrinsic photosensitivity. Science 295, 1065–70. [PubMed: 11834834]
12. Ecker JL, Dumitrescu ON, Wong KY, Alam NM, Chen SK, LeGates T, Renna JM, Prusky GT, Berson DM, and Hattar S (2010). Melanopsin-Expressing Retinal Ganglion-Cell Photoreceptors: Cellular Diversity and Role in Pattern Vision. Neuron 67, 49–60. [PubMed: 20624591]
13. Hughes S, Jagannath A, Rodgers J, Hankins MW, Peirson SN, and Foster RG (2016). Signalling by melanopsin (OPN4) expressing photosensitive retinal ganglion cells. Eye 30, 247–254. [PubMed: 26768919]
14. Schmidt TM, Do MT, Dacey D, Lucas R, Hattar S, and Matynia A (2011). Melanopsin-positive intrinsically photosensitive retinal ganglion cells: from form to function. J. Neurosci 31, 16094–16101. [PubMed: 22072661]
15. Schmidt TM, Chen SK, and Hattar S (2011). Intrinsically photosensitive retinal ganglion cells: many subtypes, diverse functions. Trends Neurosci 34, 572–580. [PubMed: 21816493]
16. Bailes HJ, and Lucas RJ (2010). Melanopsin and inner retinal photoreception. Cell. Mol. Life Sci 67, 99–111. [PubMed: 19865798]
17. Do MT, and Yau KW (2010). Intrinsically photosensitive retinal ganglion cells. Physiol. Rev 90, 1547–1581. [PubMed: 20959623]
18. Hankins MW, Peirson SN, and Foster RG (2008). Melanopsin: an exciting photopigment. Trends Neurosci 31, 27–36. [PubMed: 18054803]
19. Nayak KS, Jegla T, and Panda S (2007). Role of a novel photopigment, melanopsin, in behavioral adaptation to light. Cell. Mol. Life Sci 64, 144–154. [PubMed: 17160354]
20. Rupp A, Schmidt TM, Chew K, Yungher B, Park K, and Hattar S (2013). IpRGCs mediate ipsilateral pupil constriction. Invest. Ophthalmol. Vis. Sci 54, 310.

21. Schmidt TM, Rupp AC, Chew KS, Yungher B, Cui Y, Wess J, Park K, and Hattar S (2014). A retinal projection to the iris mediates pupil constriction. Invest. Ophthalmol. Vis. Sci 55, 1231. [PubMed: 24591482]
22. Semo M, Gias C, Ahmado A, and Vugler A (2014). A role for the ciliary marginal zone in the melanopsin-dependent intrinsic pupillary light reflex. Exp. Eye Res 119, 8–18. [PubMed: 24316157]
23. Do MT, Kang SH, Xue T, Zhong H, Liao HW, Bergles DE, and Yau KW (2009). Photon capture and signalling by melanopsin retinal ganglion cells. Nature 457, 281–287. [PubMed: 19118382]
24. Samuel U, Lutjen-Drecoll E, and Tamm ER (1996). Gap junctions are found between iris sphincter smooth muscle cells but not in the ciliary muscle of human and monkey eyes. Exp Eye Res 63, 187–192. [PubMed: 8983976]
25. Daniel EE, Tomita T, Tsuchida S, & Watanabe M (1992). Sphincters: normal function-changes in diseases (CRC Press), pp. 346–348.
26. Wolf KV (1987). Light and electron microscopic studies regarding cell contractility and cell coupling in light sensitive smooth muscle cells from the isolated frog iris sphincter. Zeitschrift für Naturforsch C 42, 977–985.
27. Juszczak GR, and Swiergiel AH (2009). Properties of gap junction blockers and their behavioural, cognitive and electrophysiological effects: animal and human studies. Prog. Neuro-Psychopharmacology Biol. Psychiatry 33, 181–198.
28. Abrams P, Andersson K-E, Buccafusco JJ, Chapple C, Groat WC, Fryer AD, Kay G, Laties A, Nathanson NM, Pasricha PJ, et al. (2006). Muscarinic receptors: their distribution and function in body systems, and the implications for treating overactive bladder. Br. J. Pharmacol 148, 565–578. [PubMed: 16751797]
29. Ishii M, and Kurachi Y (2006). Muscarinic acetylcholine receptors. Curr. Pharm. Des 12, 3573–3581. [PubMed: 17073660]
30. Matsui M, Motomura D, Karasawa H, Fujikawa T, Jiang J, Komiya Y, Takahashi S, and Taketo MM (2000). Multiple functional defects in peripheral autonomic organs in mice lacking muscarinic acetylcholine receptor gene for the M3 subtype. Proc. Natl. Acad. Sci 97, 9579–84. [PubMed: 10944224]
31. Matsui M, Motomura D, Fujikawa T, Jiang J, Takahashi S, Manabe T, and Taketo MM (2002). Mice lacking M_2 and M_3 muscarinic acetylcholine receptors are devoid of cholinergic smooth muscle contracts but still viable. J. Neurosci 22, 10627–10632. [PubMed: 12486155]
32. Engelund A, Fahrenkrug J, Harrison A, and Hannibal J (2010). Vesicular glutamate transporter 2 (VGLUT2) is co-stored with PACAP in projections from the rat melanopsin-containing retinal ganglion cells. Cell Tissue Res 340, 243–255. [PubMed: 20339872]
33. Engelund A, Fahrenkrug J, Harrison A, Luuk H, and Hannibal J (2012). Altered pupillary light reflex in PACAP receptor 1-deficient mice. Brain Res 1453, 17–25. [PubMed: 22459045]
34. Xin H-B, Deng KY, Rishniw M, Ji G, and Kotlikoff MI (2002). Smooth muscle expression of Cre recombinase and eGFP in transgenic mice. Physiol. Genomics 10, 211–215. [PubMed: 12209023]
35. Hatori M, Le H, Vollmers C, Keding SR, Tanaka N, Schmedt C, Jegla T, and Panda S (2008). Inducible ablation of melanopsin-expressing retinal ganglion cells reveals their central role in non-image forming visual responses. PLoS One 3, e2451. [PubMed: 18545654]
36. Madisen L, Zwingman TA, Sunkin SM, Oh SW, Zariwala HA, Gu H, Ng LL, Palmiter RD, Hawrylycz MJ, and Jones AR (2010). A robust and high-throughput Cre reporting and characterization system for the whole mouse brain. Nat. Neurosci 13, 133–140. [PubMed: 20023653]
37. Badea TC, Hua ZL, Smallwood PM, Williams J, Rotolo T, Ye X, and Nathans J (2009). New mouse lines for the analysis of neuronal morphology using CreER (T)/loxP-directed sparse labeling. PLoS One 4, e7859. [PubMed: 19924248]
38. Lai YL (1972). The development of the sphincter muscle in the iris of the albino rat. Exp. Eye Res 14, 196–202. [PubMed: 4640867]
39. Davis-Silberman N, and Ashery-Padan R (2008). Iris development in vertebrates; genetic and molecular considerations. Brain Res 1192, 17–28. [PubMed: 17466284]

40. Davis-Silberman N, Kalich T, Oron-Karni V, Marquardt T, Kroeber M, Tamm ER, and Ashery-Padan R (2005). Genetic dissection of Pax6 dosage requirements in the developing mouse eye. Hum. Mol. Genet 14, 2265–2276. [PubMed: 15987699]
41. Rezai KA, Lappas A, Farrokh-Siar L, Kohen L, Wiedemann P, and Heimann K (1997). Iris pigment epithelial cells of long evans rats demonstrate phagocytic activity. Exp. Eye Res 65, 23–29. [PubMed: 9237861]
42. Vugler A, Joseph A, and Jeffery G (2008). Survival and remodeling of melanopsin cells during retinal dystrophy. Vis. Neurosci 25, 125–138. [PubMed: 18442436]
43. Hubbard KB, and Hepler JR (2006). Cell signalling diversity of the Gqα family of heterotrimeric G proteins. Cell. Signal 18, 135–150. [PubMed: 16182515]
44. Offermanns S (1999). New insights into the in vivo function of heterotrimeric G-proteins through gene deletion studies. Naunyn. Schmiedebergs. Arch. Pharmacol 360, 5–13. [PubMed: 10463328]
45. Offermanns S (2001). *In vivo* functions of heterotrimeric G-proteins: studies in Galpha-deficient mice. Oncogene 20, 1635–1642. [PubMed: 11313911]
46. Chew KS, Schmidt TM, Rupp AC, Kofuji P, and Trimarchi JM (2014). Loss of G q/11 Genes Does Not Abolish Melanopsin Phototransduction. PLoS One 9, e98356. [PubMed: 24870805]
47. Hughes S, Jagannath A, Hickey D, Gatti S, Wood M, Peirson SN, Foster RG, and Hankins MW (2014). Using siRNA to define functional interactions between melanopsin and multiple G Protein partners. Cell. Mol. Life Sci 72, 165–179. [PubMed: 24958088]
48. Berridge MJ (2008). Smooth muscle cell calcium activation mechanisms. J. Physiol 586, 5047–5061. [PubMed: 18787034]
49. Taylor CW, Genazzani AA, and Morris SA (1999). Expression of inositol trisphosphate receptors. Cell Calcium 26, 237–251. [PubMed: 10668562]
50. Wang Y, Chen J, Wang Y, Taylor CW, Hirata Y, Hagiwara H, Mikoshiba K, Toyo-oka T, Omata M, and Sakaki Y (2001). Crucial role of type 1, but not type 3, inositol 1, 4, 5-trisphosphate (IP3) receptors in IP3-induced Ca2+ release, capacitative Ca2+ entry, and proliferation of A7r5 vascular smooth muscle cells. Circ. Res 88, 202–209. [PubMed: 11157673]
51. Vugler A, Semo M, Ortín-Martínez A, Rojanasakul A, Nommiste B, Valiente-Soriano FJ, García-Ayuso D, Coffey P, Vidal-Sanz M, and Gias C (2015). A role for the outer retina in development of the intrinsic pupillary light reflex in mice. Neuroscience 286, 60–78. [PubMed: 25433236]
52. Fisahn A, Yamada M, Duttaroy A, Gan JW, Deng CX, McBain CJ, and Wess J (2002). Muscarinic induction of hippocampal gamma oscillations requires coupling of the M1 receptor to two mixed cation currents. Neuron 33, 615–624. [PubMed: 11856534]
53. Yamada M, Miyakawa T, Duttaroy A, Yamanaka A, Moriguchi T, Makita R, Ogawa M, Chou CJ, Xia B, and Crawley JN, et al. (2001). Mice lacking the M3 muscarinic acetylcholine receptor are hypophagic and lean. Nature 410, 207–212. [PubMed: 11242080]
54. Offermanns S, Hashimoto K, Watanabe M, Sun W, Kurihara H, Thompson RF, Inoue Y, Kano M, and Simon MI (1997). Impaired motor coordination and persistent multiple climbing fiber innervation of cerebellar Purkinje cells in mice lacking Gαq. Proc. Natl. Acad. Sci 94, 14089–14094. [PubMed: 9391157]
55. Offermanns S, Zhao L, Gohla A, Sarosi I, Simon MI, and Wilkie TM (1998). Embryonic cardiomyocyte hypoplasia and craniofacial defects in Gαq. Gα11-mutant mice. EMBO J 17, 4304–4312. [PubMed: 9687499]
56. Xu X, Croy JT, Zeng W, Zhao L, Davignon I, Popov S, Yu K, Jiang H, Offermanns S, and Muallem S (1998). Promiscuous coupling of receptors to Gq class α subunits and effector proteins in pancreatic and submandibular gland cells. J. Biol. Chem 273, 27275–27279. [PubMed: 9765251]
57. Kim D, Jun KS, Lee SB, Kang NG, Kim YH, Ryu SH, Suh PG, and Shin HS (1997). Phospholipase C isozymes selectively couple to specific neurotransmitter receptors. Nature 389, 290–293. [PubMed: 9305844]
58. Jiang H, Kuang Y, Wu Y, Xie W, Simon MI, and Wu D (1997). Roles of phospholipase C β2 in chemoattractant-elicited responses. Proc. Natl. Acad. Sci 94, 7971–7975. [PubMed: 9223297]
59. Xie W, Samoriski GM, McLaughlin JP, Romoser VA, Smrcka A, Hinkle PM, Bidlack JM, Gross RA, Jiang H, and Wu D (1999). Genetic alteration of phospholipase C β3 expression modulates

behavioral and cellular responses to μ opioids. Proc. Natl. Acad. Sci 96, 10385–10390. [PubMed: 10468617]

60. Jiang H, Lyubarsky A, Dodd R, Vardi N, Pugh E, Baylor D, Simon MI, and Wu D (1996). Phospholipase C β4 is involved in modulating the visual response in mice. Proc. Natl. Acad. Sci 93, 14598–14601. [PubMed: 8962098]
61. Matsumoto M, Nakagawa T, Inoue T, and Nagata E (1996). Ataxia and epileptic seizures in mice lacking type 1 inositol 1, 4, 5-trisphosphate receptor. Nature 379, 168. [PubMed: 8538767]
62. Futatsugi A, Nakamura T, Yamada MK, Ebisui E, Nakamura K, Uchida K, Kitaguchi T, Takahashi-Iwanaga H, Noda T, Aruga J, et al. (2005). IP_3 Receptor Types 2 and 3 Mediate Exocrine Secretion Underlying Energy Metabolism. Science 309, 2232–2234. [PubMed: 16195467]

Highlights

- The pupillary light reflex of many sub-primates has a mechanism intrinsic to the iris
- The mouse iris sphincter is photosensitive, independent of synaptic transmission
- Deleting melanopsin in sphincter muscle removes its intrinsic photosensitivity
- The components of the melanopsin photosignaling in sphincter muscle are revealed

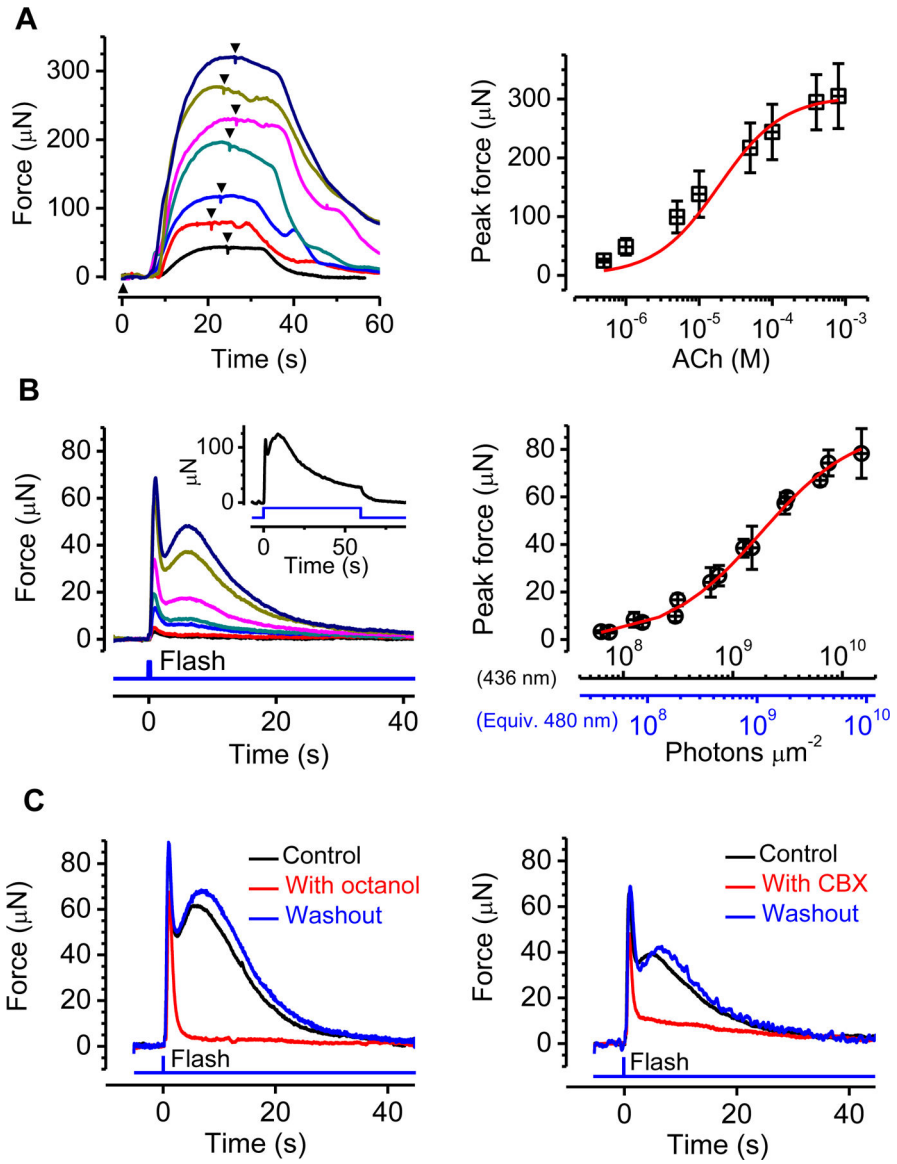

Figure 1. ACh- and Light-Induced Contraction of Isolated Mouse Iris Sphincter Muscle.

(**A**) Left, Force responses of sphincter muscle to steps of bath-applied ACh (1, 5, 10, 50, 100, 400, and 800 μM). Traces are arbitrarily aligned at the onset of ACh (upward arrowhead). Downward arrowheads indicate the offset of bath applied ACh. Right, averaged data measured at response peak (mean ± SD, n = 6), and fitted with Hill equation (red curve) with $K_{1/2}$ of 18.7 μM and Hill coefficient (n_H) of 1.0. (**B**) Left, Force responses of sphincter muscle to light flashes (6.27×10^7, 1.25×10^8, 3.14×10^8, 6.27×10^8, 1.25×10^9, 3.14×10^9, and 6.27×10^9 photons μm^{-2} at 436 nm). Flashes were 10–300 msec in duration. Inset, sample response to a 60-sec step of light (3.08×10^9 photons μm^{-2} sec^{-1} at 436 nm). Right, averaged data at initial peak of the force response (mean ± SD, each data point represents mean amplitude from 3 muscles; 6 muscles were tested), fitted with Hill equation (red curve) with $I_{1/2}$ of 1.8×10^9 photons μm^{-2} at 436 nm and n_H of 1.0. Flash intensities in this panel are expressed also in equivalent photons at 480 nm, λ_{max} of melanopsin. (**C**)

Effects of gap-junction blockers. Left, 500-μM octanol. Right, 200-μM CBX. In both, light flash delivered 7.38×10^9 photons μm^{-2} at 436 nm. Three experiments on octanol and 2 experiments on CBX gave similar results. Recording traces in all panels are from single trials, with light monitor given below. The Hill-equation fits in (**A**) and (**B**) are purely empirical, so we do not interpret n_H further.
See also Figure S1

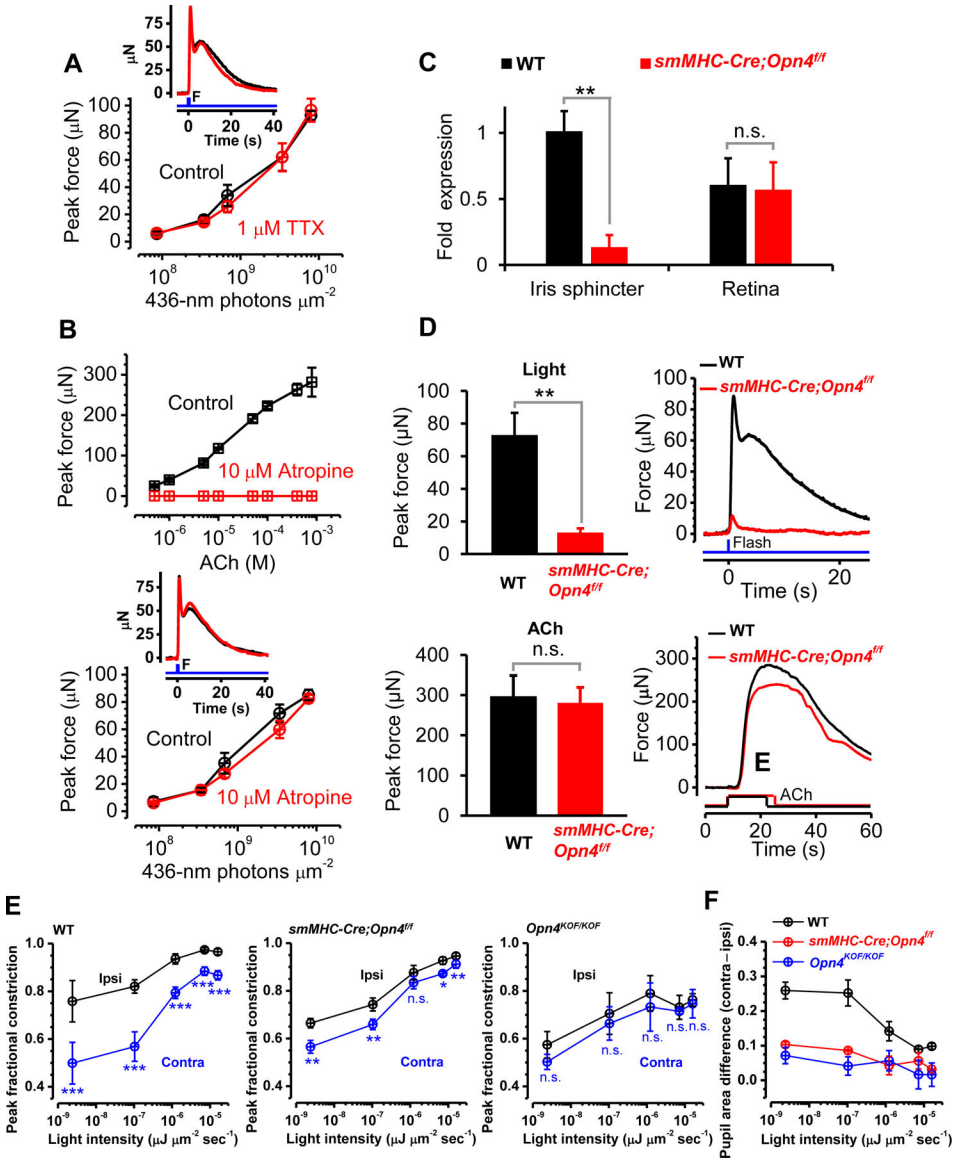

Figure 2. Pharmacological Experiments on Isolated Sphincter Muscle, and Smooth-Muscle-Specific Knockout of Melanopsin.

(**A**) Collected and averaged flash intensity-response relation of isolated WT sphincter muscle with (red) and without (black) TTX (mean ± SD, n = 3). Initial response peak plotted. Inset, sample responses of an isolated WT iris sphincter muscle to a bright flash (7.95×10^9 photons μm^{-2} at 436 nm) before (black) and during application of 1-μM TTX (red). (**B**) Top, 10-μM atropine completely blocked WT muscle's response to ACh (mean ± SD, n = 3). Bottom, atropine had no effect on flash response of muscle to ACh (mean ± SD, n = 3). Inset, sample flash response in the absence or presence of atropine; 7.95×10^9 photons μm^{-2} at 436 nm. (**C**) Relative expression of *Opn4* in the iris sphincter region and the retina isolated from *smMHC-Cre;Opn4*$^{f/f}$ (mean ± SD, n=3) and WT (mean ± SD, n=3) mice, with the WT message level in sphincter region arbitrarily assigned as unity. ** $P < 0.01$, when *Opn4* mRNA of *smMHC-Cre;Opn4*$^{f/f}$ iris sphincter or retina was compared to corresponding WT value by unpaired two-sample *t*-test. n.s. $P > 0.05$. (**D**) Top left, averaged

peak amplitude of flash-induced tension for iris sphincter muscle isolated from WT versus *smMHC-Cre;Opn4*$^{f/f}$ mice (mean ± SD, n = 3 each). ** $P < 0.01$, by unpaired two-sample *t*-test. Top right, sample response of WT and *smMHC-Cre;Opn4*$^{f/f}$ muscles to a bright flash (8.61×10^9 photons μm^{-2} at 436 nm). Recording traces are from single trials. Bottom left, averaged peak amplitude of 800-μM ACh-induced tension for WT and *smMHC-Cre;Opn4*$^{f/f}$ iris sphincter muscles (mean ± SD, n = 3 each). n.s. $P > 0.05$, by unpaired two-sample *t*-test. Bottom right, sample response of WT and *smMHC-Cre;Opn4*$^{f/f}$ iris sphincter muscles to a step of 800-μM ACh. Single trials. (**E**) *In vivo* overall PLR (peak fractional constriction = $(A_{dark} - A_{light})/A_{dark}$) intensity-response relations, obtained with monocular illumination, from ipsilateral (stimulated) eye and contralateral (unstimulated) eye for WT (mean ± SD, n = 4), *smMHC-Cre;Opn4*$^{f/f}$ (mean ± SD, n = 3), and *Opn4*$^{KOF/KOF}$ mice (mean ± SD, n = 3). 505-nm light step used. See STAR METHODS. * $P < 0.05$, ** $P < 0.01$, *** $P < 0.001$, when overall PLR was compared between contralateral eye and ipsilateral value by using paired two-sample *t*-test. n.s. $P > 0.05$. (**F**) Difference in pupil area between ipsilateral and contralateral eye calculated from (**E**).

See also Figure S2–S3.

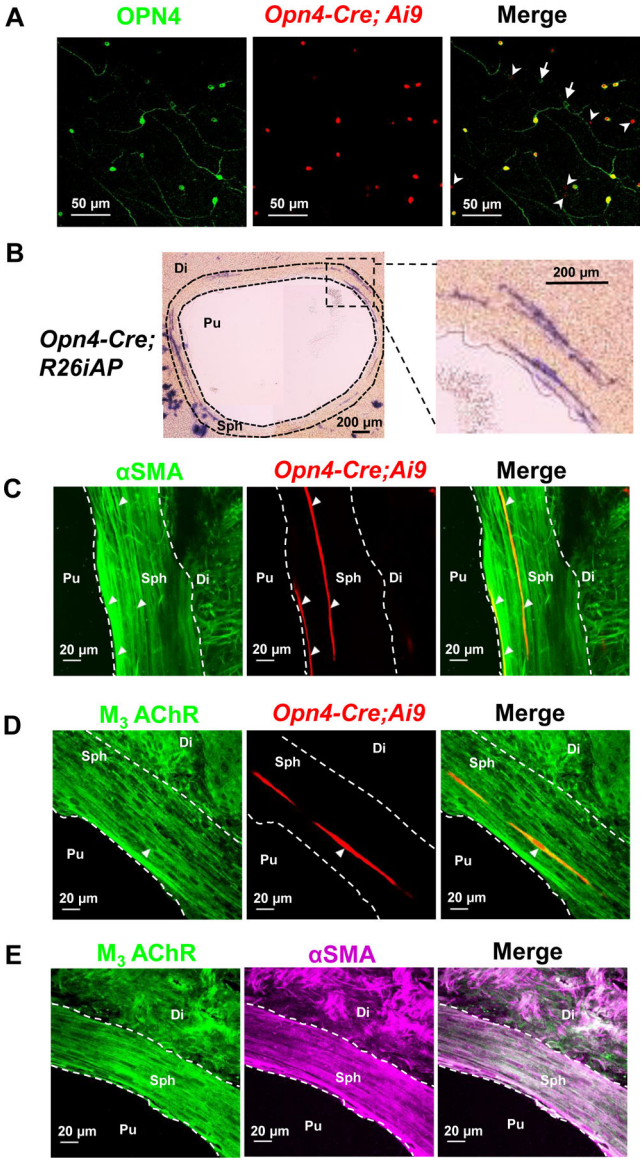

Figure 3. Melanopsin Expression in Mouse Iris.

(**A**) Flat-mount *Opn4-Cre;Ai9* retina immunostained for melanopsin (OPN4, green) for verifying the specificity of genetic-labeling. Red indicates fluorescence directly from tdTomato. In the merged panel, arrowheads mark tdTomato-positive but melanopsin-immunonegative cells; arrows mark melanopsin-immunopositive but tdTomato-negative cells. (**B**) Flat-mount *Opn4-Cre;R26iAP* iris stained for alkaline phosphatase (purple). Boxed area on left is enlarged on right to show morphology of labeled cells. (**C**) Flat-mount *Opn4-Cre;Ai9* (red) iris immunostained for α-smooth muscle actin (αSMA, green). Arrowheads mark tdTomato-positive sphincter muscle cells. (**D**) Flat-mount *Opn4-Cre;Ai9* (red) iris immunostained for M_3 muscarinic acetylcholine receptor (M_3-AChR, green). (**E**) Flat-mount WT mouse iris immunostained for M_3-AChR (green) and αSMA (magenta). Dotted lines in (**B**)-(**E**) demarcate the pupil (Pu), sphincter muscle (Sph) and dilator muscle (Di).

See also Figure S4.

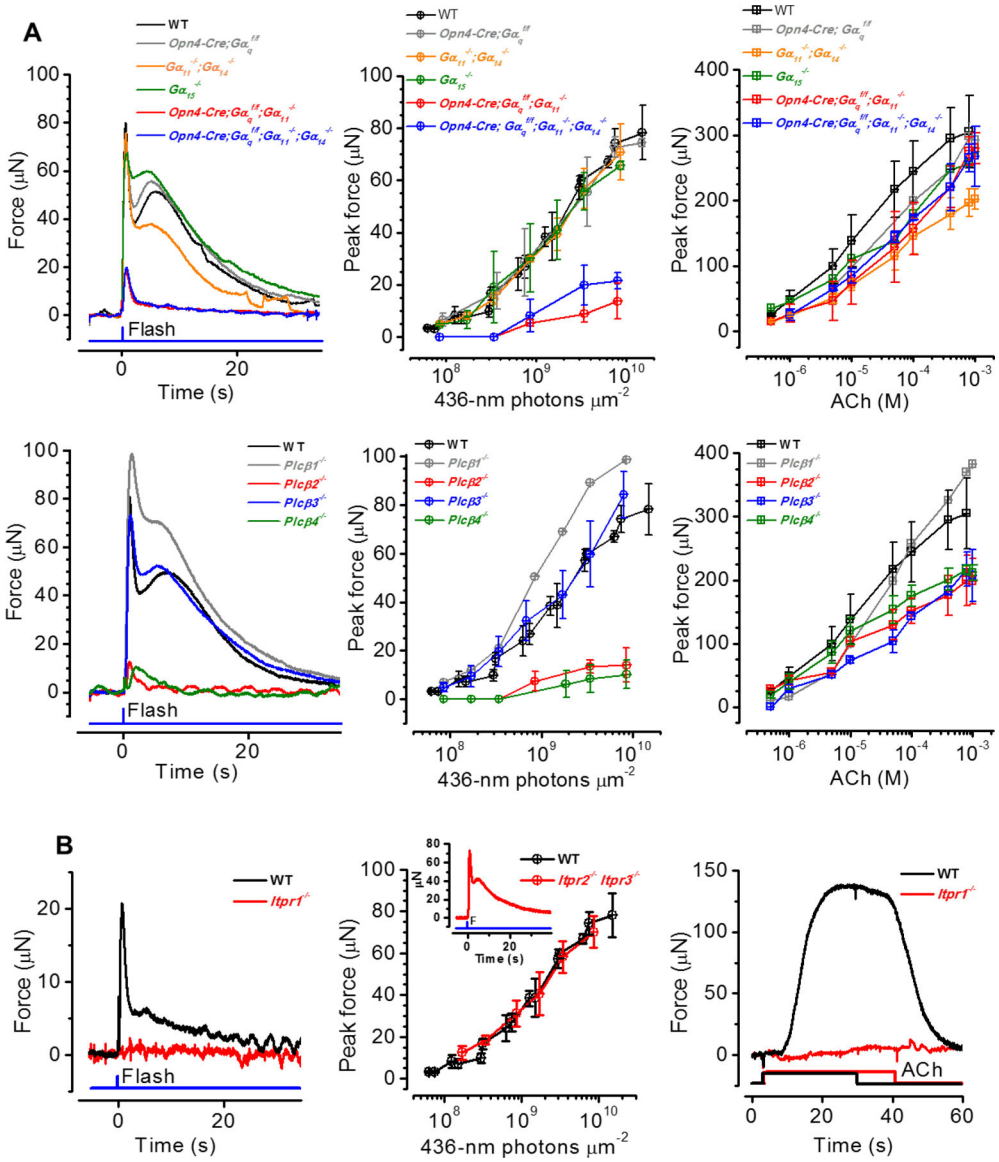

Figure 4. Shared Signaling Mechanism for Light-Activated and ACh-Activated Contraction of Iris Sphincter Muscle.

(**A**) Top left, sample responses to a light flash (7.95×10^9 photons μm^{-2} at 436nm) by iris sphincter muscles from WT, *Opn4-Cre;*$Ga_q^{f/f}$, $Ga_{11}^{-/-};Ga_{14}^{-/-}$, $Ga_{15}^{-/-}$, *Opn4-Cre;*$Ga_q^{f/f};Ga_{11}^{-/-}$ and O*pn4-Cre;*$Ga_q^{f/f};Ga_{11}^{-/-};Ga_{14}^{-/-}$ mice. Top middle, flash intensity-response relations of WT (reproduced from Figure 1B), *Opn4-Cre;*$Ga_q^{f/f}$ (mean ± SD, 3 muscles), $Ga_{11}^{-/-};Ga_{14}^{-/-}$ (mean ± SD, 3 muscles), $Ga_{15}^{-/-}$ (mean ± SD, 3 muscles), *Opn4-Cre;*$Ga_q^{f/f};Ga_{11}^{-/-}$ (mean ± SD, 3 muscles) and *Opn4-Cre;*$Ga_q^{f/f};Ga_{11}^{-/-};Ga_{14}^{-/-}$ muscles (mean ± SD, 3 muscles). Top right, ACh dose-response relation of WT (same as in Figure 1A), *Opn4-Cre;*$Ga_q^{f/f}$ (mean ± SD, 2 muscles), $Ga_{11}^{-/-};Ga_{14}^{-/-}$ (mean ± SD, 4 muscles), $Ga_{15}^{-/-}$ (1 muscle), *Opn4-Cre;*$Ga_q^{f/f};Ga_{11}^{-/-}$ (mean ± SD, 3 muscles) and *Opn4-Cre;*$Ga_q^{f/f};Ga_{11}^{-/-};Ga_{14}^{-/-}$ muscles (mean ± SD, 2 muscles). Bottom left, sample responses of iris sphincter muscles from $Plc\beta1^{-/-}$, $Plc\beta2^{-/-}$, $Plc\beta3^{-/-}$ and $Plc\beta4^{-/-}$ mice to a light flash (8.52×10^9 photons μm^{-2} at 436nm). Bottom middle, flash

intensity-response relations for WT (same as in Figure 1B), *Plcβ1*$^{-/-}$ (1 muscle, owing to limited animal availability; it showed a larger light response than WT possibly due to an older animal age of 2 years), *Plcβ2*$^{-/-}$ (mean ± SD, 4 muscles), *Plcβ3*$^{-/-}$ (mean ± SD, 3 muscles) and *Plcβ4*$^{-/-}$ muscles (mean ± SD, 2 muscles). Bottom right, ACh dose-response relation of WT (same as in Figure 1A), *Plcβ1*$^{-/-}$ (1 muscle, from 2-year-old animal), *Plcβ2*$^{-/-}$ (mean ± SD, 3 muscles), *Plcβ3*$^{-/-}$ (mean ± SD, 3 muscles) and *Plcβ4*$^{-/-}$ muscles (mean ± SD, 4 muscles). (**B**) Left, sample flash responses of a WT (from P23 animal) and an *Itpr1*$^{-/-}$ (from P23 animal) sphincter muscles. The younger age was chosen because of survival issue with *Itpr1*$^{-/-}$ animals, hence same with WT for proper comparison. 8.52×10^{9} photons μm^{-2} at 436nm. 3 experiments gave similar results. Middle, flash intensity-response relations for WT (same as in Figure 1B) and *Itpr2*$^{-/-}$;*Itpr3*$^{-/-}$ muscles (mean ± SD, 3 muscles). Inset shows sample light response of *Itpr2*$^{-/-}$;*Itpr3*$^{-/-}$ iris (7.95×10^{9} photons μm^{-2} at 436nm). Right, sample responses to 50-μM ACh by WT (from P23 animal) and *Itpr1*$^{-/-}$ (from P23 animal) iris sphincter muscles. Note the same onset but different offset times of bath-applied ACh, indicated by the black (WT) and red (*Itpr1*$^{-/-}$) traces. 3 experiments gave similar results. Recording traces are from single trials, with light monitor given below.

KEY RESOURCES TABLE

REAGENT or RESOURCE	SOURCE	IDENTIFIER
Antibodies		
Rabbit polyclonal anti-Melanopsin	Advanced Targeting Systems	Cat#AB-N38; RRID:AB_1608077
Goat polyclonal antibody anti-α-smooth muscle actin	AbCam	Cat#ab21027; RRID: AB_1951138
Rabbit polyclonal anti-M3 muscarinic receptor	Research and Diagnostics Antibodies	Cat# AS3741S
Rabbit polyclonal anti-PAX6	Covance	Cat#PRB-278P
Chemicals, Peptides, and Recombinant Proteins		
Ames' medium	Sigma-Aldrich	Cat#A1420
Acetylcholine chloride	Sigma-Aldrich	Cat#A6625
Atropine	Sigma-Aldrich	Cat#A0132
DNQX	Sigma-Aldrich	Cat#D0540
DL-2-amino-5-phosphonopentanoic acid	Sigma-Aldrich	Cat#A5282
DL-2-Amino-4-phosphonobutyric acid	Sigma-Aldrich	Cat#A1910
Tetrodotoxin	Alomone labs	Cat#T-500
L-Glutamic acid	Sigma-Aldrich	Cat#49449
PACAP 1–27	Tocris	Cat#1183
PACAP 1–38	Tocris	Cat#1186
PACAP 6–38	Tocris	Cat#3236
Octanol	Sigma-Aldrich	Cat#112615
Carbenoxolone disodium salt	Sigma-Aldrich	Cat#C4790
Critical Commercial Assays		
VECTOR Blue Alkaline Phosphatase Substrate Kit	Vector Laboratories	Cat#5300; RRID: AB_2336837
Deposited Data		
Experimental Models: Cell Lines		
Mouse embryonic stem cell: EPD0642_3_D12 (*Opn4*$^{tm1a(KOMP)Wtsi}$)	UCDAVIS KOMP Repository	Project ID: CSD82970
Experimental Models: Organisms/Strains		
Mouse: C57BL/6J	The Jackson Laboratory	Cat#000664; RRID:IMSR_JAX:000664
Mouse: B6(Cg)-*Tyr*$^{c-2J}$/J	The Jackson Laboratory	Cat#000058
Mouse: *Chrm1*$^{-/-}$;*Chrm3*$^{-/-}$	[52,53]	N/A
Mouse: $Gα_q^{f/f}$	[54]	N/A
Mouse: $Gα_{11}^{-/-}$	[55]	N/A
Mouse: $Gα_{14}^{-/-}$	[56]	N/A
Mouse: $Gα_{15}^{-/-}$	[56]	N/A
Mouse: *Plcβ1*$^{-/-}$	[57]	N/A
Mouse: *Plcβ2*$^{-/-}$	[58]	N/A
Mouse: *Plcβ3*$^{-/-}$	[59]	N/A

REAGENT or RESOURCE	SOURCE	IDENTIFIER
Mouse: *Plcβ4*$^{-/-}$	[60]	N/A
Mouse: *Itpr1*$^{-/-}$	[61]	N/A
Mouse: *Itpr2*$^{-/-}$;*Itpr3*$^{-/-}$	[62]	N/A
Mouse: *smMHC-Cre*: B6.Cg-Tg(Myh11-cre,-EGFP)2Mik/J	The Jackson Laboratory	Cat# JAX:007742; RRID:IMSR_JAX:007742
Mouse: *Opn4*$^{f/f}$	This paper	N/A
Mouse: *Opn4*$^{KOF/KOF}$	This paper	N/A
Mouse: *Opn4-Cre*	This paper	N/A
Mouse: ACTB:FLPe B6J	The Jackson Laboratory	Cat# JAX:005703; RRID:IMSR_JAX:005703
Oligonucleotides		
Genotyping primer: *Opn4*$^{f/f}$ Forward: 5'-TCT ACA CAG TGG CTG AGA CAA GAG G-3' Reverse: 5'- AAG AGG GAG TGA AAG GCT CAG ATG G-3'	This paper	N/A
Genotyping primer: *Opn4-Cre* Forward: 5'- TGT GAA GGA CAG AGC CTC CT −3' Reverse: 5'- CAG CCC GGA CCG ACG ATG AAG −3'	This paper	N/A
Primers for *Opn4S* Forward: 5'-GCT ACC GCT CTA CCC ACC −3' Reverse: 5'- CTA CAT CCC GAG ATC CAG ACT G-3'	This paper	N/A
Primers for *Opn4L* Forward: 5'- GCT ACC GCT CTA CCC ACC −3' Reverse: 5'- CAC CTT GGG AGT CTT AGA TCT CTG −3'	This paper	N/A
Primers for *Opn4* Forward: 5'-TAG CCC CAC GAC ATC TGC A-3' Reverse: 5'- GTA GAG GCT GCT GGC AAA GA −3'	This paper	N/A
Primers for *β-actin* Forward: 5'- AAA GAG AAG CTG TGC TAT GTT G −3' Reverse: 5'- CAT AGA GGT CTT TAC GGA TGT C −3'	This paper	N/A
Recombinant DNA		
Bacterial artificial chromosome (BAC) clone: RP23–340N18	BACPAC Resource Center	N/A